I.J. Image, Graphics and Signal Processing, **2026, 2, 36-50**
Published Online on April 8, 2026 by MECS Press (http://www.mecs-press.org/)
DOI: 10.5815/ijigsp.2026.02.03

Scaling of Digital Images by Adaptive and Combined Application of Interpolation Algorithms

Serhiy Balovsyak*
Yuriy Fedkovych Chernivtsi National University, Chernivtsi, 58012, Ukraine
E-mail: s.balovsyak@chnu.edu.ua
ORCID iD: https://orcid.org/0000-0002-3253-9006
*Corresponding Author

Mariana Borcha
Yuriy Fedkovych Chernivtsi National University, Chernivtsi, 58012, Ukraine
E-mail: m.borcha@chnu.edu.ua
ORCID iD: https://orcid.org/ 0000-0001-6758-3173

Yurii Hnatiuk
Yuriy Fedkovych Chernivtsi National University, Chernivtsi, Ukraine
E-mail: hnatiuk.yurii@chnu.edu.ua
ORCID iD: https://orcid.org/0009-0006-5605-9281

Khrystyna Odaiska
Yuriy Fedkovych Chernivtsi National University, Chernivtsi, Ukraine
E-mail: k.odaiska@chnu.edu.ua
ORCID iD: https://orcid.org/0000-0002-3167-1195

Ihor Fodchuk
Yuriy Fedkovych Chernivtsi National University, Chernivtsi, Ukraine
E-mail: i.fodchuk@chnu.edu.ua
ORCID iD: https://orcid.org/0000-0001-6772-6920

Received: 09 August, 2025; Revised: 07 December, 2025; Accepted: 21 January, 2026; Published: 08 April, 2026

Abstract: The article describes the theoretical foundations and software tools for scaling digital images by adaptive and combined application of bilinear and bicubic interpolation algorithms. An analysis of modern algorithms and image scaling tools has been performed. The theoretical foundations of image scaling using interpolation algorithms are described. The root mean square error between the pixel values of the original and scaled images was used as the scaling error. The scaling of images was performed by a complex of two interpolation algorithms. The first algorithm reduces the image scale, after which the second algorithm increases the scale. Such image processing is performed, in particular, in telecommunication systems for transmitting images at reduced scales. A correlation was found between the values of the average spatial period of the image and the relative scaling error, which is equal to the ratio of the scaling errors for different interpolation algorithms. The spatial period of the image was calculated based on its energy spectrum. A regression analysis was performed to determine the dependence of the relative scaling error on the spatial period of the images. It is found that in most cases bicubic interpolation provides a smaller scaling error, but for some images with small spatial period, bilinear interpolation provides a smaller error. It is proposed to increase the scaling accuracy by adaptively selecting the image interpolation algorithm depending on its spatial period. A combined application of interpolation algorithms was performed, which consists of reducing the scale using the bilinear interpolation algorithm and increasing the scale using the bicubic interpolation algorithm. A statistical analysis of the results of image scaling was performed. It was found that the combined application of algorithms in most cases provides a smaller error than the separate application of the bicubic and bilinear interpolation algorithms.

Index Terms: Scaling Of Digital Images, Interpolation Algorithms, Regression Analysis, Software, Spatial Period of Images

This work is open access and licensed under the Creative Commons CC BY 4.0 License.

1. Introduction

Scaling of digital images is often applied in modern computer systems when processing both separate images and video stream frames [1, 2]. Scaling down of images involves reducing their dimensions (in pixels) and is used, for example, to reduce memory usage, unify a series of images to a single size, or decrease traffic of telecommunication system channels. Scaling up of images involves increasing their dimensions and is applied, for instance, to enhance visualization or restore images to their original size. Scaling of digital raster images is reduced to changing the sampling frequency for a discrete signal [3]. Changing the resolution of images is performed in various video surveillance and computer graphics systems. In scientific research, the task of image scaling arises during the processing of biomedical images [4, 5], X-ray images [6], and electron diffraction images [7]. Transformation to a specified scale is used as a pre-processing stage in computer systems for image recognition and detection [8, 9]. Since image scaling has a wide range of applications, there is currently a need to develop accurate and fast tools for changing image resolution.

Modern hardware and software tools for image scaling in most cases use interpolation algorithms that have high performance and relative simplicity of software or hardware implementation. The most common algorithms based on linear image interpolation include: nearest neighbor, Lanczos, bilinear and bicubic interpolation [3, 10]. Nonlinear image interpolation algorithms, for example, Weighted Essentially Non-Oscillatory (WENO), provide contour preservation and reduce aliasing effects [11]. In general, nonlinear image interpolation algorithms provide higher subjective quality compared to linear algorithms. However, nonlinear interpolation algorithms are characterized by higher computational complexity.

Image scaling algorithms using Fourier transform [2] and multiscale processing [12] are more complex to implement and have lower performance. A promising direction for image scaling is the use of Artificial Neural Networks (ANN), which can provide high visual quality in the resulting images. In order to minimize distortions in the scaled images, the brightness and contrast values of the images are corrected (if necessary) [13].

The possibilities of image scaling using the Pyramid Image and on Spline Model of 2-6 orders are discussed in [12]. The spline model provides smoothness for the brightness distribution of the original image, but the proposed model has a more complex software implementation compared to standard interpolation methods.

A novel image super-resolution algorithm based on bilateral quadratic interpolation is described in [14]. This algorithm is based on bilateral quadratic interpolation. According to the PSNR (Peak Signal to Noise Ratio) parameter, the proposed algorithm provides less distortion on the test set of images after interpolation than the standard bicubic interpolation algorithm. However, further research is needed to evaluate the performance of the bilateral quadratic interpolation algorithm on various types of images. Image upscaling is often performed using Convolutional Neural Networks (CNN) [2, 15], where the input consists of images at the initial scale, and the output provides images at an increased scale.

The basic architecture of the CNN for obtaining Super-Resolution images is SRCNN (Super-Resolution Convolutional Neural Network) [16]. The SRCNN architecture involves scaling the initial image to the desired size using the bicubic interpolation method, after which the pre-trained SRCNN model reduces the scaling defects in such an image. A modern method for improving image resolution using deep neural networks ESRGAN (Enhanced Super-Resolution Generative Adversarial Network), which provide high quality image results, is described in [2].

The study [17] describes the modern SR3 approach, according to which Super-Resolution images are obtained through Repeated Refinement. SR3 uses denoising diffusion probabilistic models to image translation, which provides photorealistic quality of scaled images. Similar to the SRCNN architecture, the SR3 approach involves scaling the original image to the desired size using bicubic interpolation. The possibilities of obtaining Super-Resolution images by jointly using deep convolutional neural networks (CNN) and transformers are considered in the work [18]. It is shown that such a combination provides high accuracy of scaled images even in the presence of noise in the original images. In [19] a novel multi-branch residual hybrid attention block (MBRHAB) is applied to improve the image scaling accuracy. Experimental studies have shown that the MBRHAB method outperforms existing Super-Resolution algorithms (including bicubic interpolation, SRCNN, ESRGAN, Real-ESRGAN) in terms of PSNR (Peak Signal-to-Noise Ratio) and SSIM (Structural Similarity Index) metrics.

Neural network image upscaling using the Spiking Neural Network (SNN) architecture is described in [20]. Unlike traditional ANN, which work with continuous signal values, SNN use discrete pulses (spikes), similar to pulses in a biological neural network. SNN provide high accuracy in image upscaling, but their training process is more complex than that of traditional ANN.

Practical application of such ANN involves training on a large set of images containing pairs of low- and high-resolution images. However, scaling images using ANN is characterized by a relatively high probability of artifacts.

There are several programs designed for image scaling using neural networks. For example, the Waifu2x program is designed to increase the scale of images by 2 or 4 times (during a single operation) [21]. The program allows processing images iteratively, that is, the original images can be rescaled. Before scaling images, users can select a processing model (e.g., "photo"), the noise reduction level (ranging from low to highest), the scaling (zoom) factor, and the size of the rectangular tile within which the processing is performed. The advantages of the Waifu2x software include the ability to reduce the noise level [22, 23] in images during the scaling process.

The analysis of the above-described literature confirms that the development of accurate and fast image scaling tools is an urgent task. Comparison of interpolation algorithms with other image scaling algorithms shows that such algorithms have a number of advantages (simplicity of implementation, high speed, low probability of artifacts). For practical applications, it is advisable to use the common bilinear and bicubic interpolation algorithms [24], since the nearest neighbor algorithm gives too high an error, and the Lanczos algorithm has a lower speed.

Thus, the use of interpolation algorithms is appropriate in cases where simplicity of implementation and high speed are important. In addition, interpolation algorithms can be successfully combined with image scaling using ANN, since in many ANN (SRCNN [16], SR3 [17]) the image scaling to the desired size is performed by the interpolation algorithm, and the ANN then reduces the scaling defects. The problem is that image interpolation algorithms have relatively low accuracy. Image scaling errors lead, in particular, to the appearance of characteristic defects, blurred contours and loss of image detail [25, 26]. At the same time, practical image processing shows that the scaling accuracy depends not only on the interpolation algorithm, but also on the type of image (for example, an image with a large or small amount of details, an image with smooth or sharp changes in the brightness gradient). Since the scaling result depends on the spatial distribution of the image brightness (or the values of its color channels), it is proposed to evaluate the image type based on its average spatial period.

In this paper, it is proposed to increase the accuracy of image scaling by adaptive and combined use of interpolation algorithms. The peculiarity of the adaptive approach is that the interpolation algorithm is selected for each image depending on its spatial period. Combined use consists in the sequential use of different interpolation algorithms when reducing and increasing the scale of one image, which is practically used when transmitting images in a reduced scale through the channels of the telecommunication system.

2. Theoretical Foundations of Image Scaling using Interpolation Algorithms

Digital color images are processed programmatically as arrays $f_{RGB}(i, k, c)$, where $i = 0,..., M-1$; $k = 0,..., N-1$; $c = 0,..., Q_C-1$; M is the image size in height (pixels), N is the image size in width (pixels), $Q_C = 3$ is the number of color channels (Red, Green, Blue) [1]. The pixel values of all color channels are converted to the range from 0 to 1. In the case of scaling an image in grayscale, it is processed as one color channel. Let us consider in more detail the main image interpolation algorithms: nearest neighbor, bilinear and bicubic interpolation, Lanczos [3].

The nearest neighbor algorithm is the simplest and consists in choosing the pixel value that is closest to the new pixel position after scaling.

According to the bilinear image interpolation algorithm, the new (scaled) pixel value is calculated through a linear combination of the values of the 4 closest pixels (to the new pixel position). When scaling images, bilinear interpolation is performed twice: along the height and along the width. Bilinear interpolation usually gives better results (compared to the nearest neighbor algorithm), but partially smooths the image.

According to the bicubic image interpolation algorithm, the new pixel value is calculated by cubic interpolation of the values of the 16 nearest pixels along two coordinates (height and width). Bicubic interpolation usually gives better results (compared to bilinear), but has a slower speed.

The Lanczos algorithm consists in calculating the new pixel value (after scaling) based on the values of neighboring pixels using the Lanczos window function (kernel). For interpolation of one-dimensional signals $s(x)$, the Lanczos kernel is described by the $sinc(x/a)$ function, where $-a \leqslant x \leqslant a$, a is the kernel size (in most cases $a = 3$). Image scaling is performed using the two-dimensional Lanczos kernel. The Lanczos algorithm has a relatively slow speed, but allows to scale images with quite high accuracy, compared to other interpolation methods.

Adaptive application of interpolation algorithms consists in using an algorithm with minimal scaling error for processing a specific image.

The following three image scaling modes can be distinguished:

1. Scaling down of all images (for example, to convert the sizes of the original images to the sizes of the input signals of the ANN).
2. Scaling up all images (e.g. before rendering images to ensure high visual quality).
3. Scaling down the original images, transmitting (or storing) such images and then scaling up them back (e.g. to reduce the amount of data transmitted in telecommunications systems; to preview images read in a reduced format; in the case of transmitting images via instant messengers).

In the first two modes, one interpolation algorithm is used (for scaling down or up). In the third mode, it is possible to use either one or a combined set of two algorithms (one algorithm is used for scaling down, and the other for scaling up).

Let us study interpolation algorithms in the most general third mode, since the first two modes are its components. In this case, image processing is reduced to 2 stages:

1. Based on the initial color image f_{RGB} ($M \times N$ pixels), interpolation algorithm # 1 calculates the scaled image f_{RGBs} ($M_s \times N_s$ pixels); the scaling factor is defined as $S_c = M_s/M$ (for example, $S_c = 0.5$).

2. Based on f_{RGBs}, interpolation algorithm # 2 calculates the resulting image f_{RGBs2} (with dimensions $M \times N$ pixels, i.e. the dimensions of the initial image).

If the scaled image f_{RGBs2} coincides with the original f_{RGB}, then the scaling error is zero (perfect scaling). However, in practice, in most cases, there is a certain difference between the images f_{RGBs2} and f_{RGB}. Therefore, to estimate the scaling error [27, 28], the difference between f_{RGBs2} and f_{RGB} is calculated as the mean square error (MSE) and as the root mean square error (RMSE) by the formulas:

$$M_{SE} = \frac{1}{M \cdot N \cdot Q_C} \sum_{i=0}^{M-1} \sum_{k=0}^{N-1} \sum_{c=0}^{Q_C-1} \left[f_{RGB}(i,k,c) - f_{RGBs2}(i,k,c) \right]^2 , \quad (1)$$

$$R_{MSE} = \sqrt{\frac{1}{M \cdot N \cdot Q_C} \sum_{i=0}^{M-1} \sum_{k=0}^{N-1} \sum_{c=0}^{Q_C-1} \left[f_{RGB}(i,k,c) - f_{RGBs2}(i,k,c) \right]^2} , \quad (2)$$

where M is the size of the f_{RGB} image in height (pixels); N is the size of the f_{RGB} image in width (pixels);

Q_C is the number of color channels.

Based on *MSE* (1), *PSNR* (Peak Signal to Noise Ratio) values are also calculated [28]. The average spatial period T_{CR} is determined for the grayscale image f_n, which is calculated based on the initial color image f_{RGB} ($M \times N$ pixels). The values of the T_{CR} period are needed to study the influence of the spatial distribution of image brightness on the scaling error *RMSE* (2). The T_{CR} period is calculated based on the Fourier energy spectrum P_S of the image f_n. To simplify the processing of the energy spectrum P_S, a square grayscale image f_n with dimensions $M_d \times N_d$ pixels is used, where $M_d = N_d = min(M, N)$. The Fourier spectrum F of the image f_n is calculated as a result of the two-dimensional direct Discrete Fourier Transform (DFT) according to the formula [29, 30]

$$F(m,n) = \sum_{i=0}^{Md-1} \sum_{k=0}^{Nd-1} f_n(i,k) \cdot \exp\left(- j \cdot 2\pi \left(\frac{m \cdot i}{M_d - 1} + \frac{n \cdot k}{N_d - 1} \right) \right), \quad (3)$$

where m is the number (index) of the spatial frequency in height (number of components of the height distribution); n is the frequency number in width; $m = 0, 1, ..., M_d - 1$; $n = 0, 1, ..., N_d - 1$; j is an imaginary unit.

To simplify the analysis of the spectrum, the origin of the variables m and n is shifted to the center of the frequency rectangle. As a result of such a shift of the origin of coordinates, the centered matrix F_C is calculated based on the matrix of Fourier spectrum coefficients F [1, 31]. The Power Spectrum (or "Power spectral density") P_S is calculated as the square of the modulus of the centered spectrum F_C using the equation

$$P_S = |F_C|^2 . \quad (4)$$

Based on the energy spectrum P_S, its averaged radial profile $P_R(d)$ is calculated, where $d = 0, 1, ..., N_R-1$, where $N_R = [M_d/2] + 1$. The radial profile $P_R(d)$ describes the dependence of the amplitudes of radial spatial frequencies (averaged for all directions) on the frequency numbers d [32]. For the energy spectrum P_S the coordinates of its center $M_C = [M_d/2]$ (in height), $N_C = [N_d/2]$ (in width) are determined.

The value of $P_R(d)$ is calculated as the arithmetic mean of the energy spectrum coefficients $P_S(m, n)$, for which $d = \left[\sqrt{(m - Mc)^2 + (n - Nc)^2} \right]$. For each number d of radial spatial frequency its value v_r is calculated

$$v_r = \frac{d}{2(N_R - 1)} . \quad (5)$$

The values of spatial frequencies v_r are in the range from 0 to 0.5 (pixels^{-1}). The average spatial frequency v_{CR} of the image f_n is calculated based on the radial profile $P_R(d)$ using the equation [33]:

$$v_{CR} = \sum_{d=d_{\min}}^{d_{\max}} v_r(d) \cdot P_R(d) \Big/ \sum_{d=d_{\min}}^{d=d_{\max}} P_R(d) , \quad (6)$$

where $v_r(d)$ is the spatial frequency value (5) corresponding to the number d; d_{min} is the minimum spatial frequency number being analyzed (e.g., $d_{min} = 1$); d_{max} is the maximum spatial frequency number being analyzed (e.g., $d_{max} = N_R$).

The values of d_{min} are chosen to be no less than 1, since $d_{min} = 0$ corresponds to the constant component of the signal. The average spatial period T_{CR} of the image is calculated as:

$$T_{CR} = \frac{1}{v_{CR}}. \tag{7}$$

The scaling errors *RMSE* are calculated separately for each set of two algorithms that are used for successive image scaling down and up. To compare the accuracy of the algorithms, the relative scaling error *RMSE_R* is also used, which is calculated as:

$$RMSE_R = \frac{RMSE_II}{RMSE_I}, \tag{8}$$

where *RMSE_I* is the scaling error by the algorithms set I; *RMSE_II* is the scaling error by the algorithms set II.

The dependence of the relative scaling error *RMSE_R* on the values of the period T_{CR} is mathematically described by a regression equation in the form of a polynomial of degree P_d:

$$RMSE_RA = b_0 + \sum_{p=1}^{Pd} b_p \cdot (T_{CR})^p, \tag{9}$$

where b_0, b_1,..., b_{Pd} are the coefficients of the polynomial.

Thus, using equation (9), it is possible to investigate the influence of the spatial period T_{CR} of images on the accuracy of their scaling.

This allows, by scaling a series of Q_{Im} test images f_{RGB}, to determine the threshold value T_h for the spatial period T_{CR} at which both sets of interpolation algorithms provide the same error; therefore, at $T_{CR} < T_h$, one of the algorithm sets provides a smaller error, and at $T_{CR} \geqslant T_h$, the other set provides a smaller error. The scaling error *RMSE* is calculated from the difference of the f_{RGB} and f_{RGBs2} images according to formula (2). After that, a regression analysis of the dependence of the relative scaling error *RMSE_R* (8) on the spatial period T_{CR} for all Q_{Im} of the studied images is performed. The regression equation is constructed in the form of a polynomial of degree P_d according to formula (9), the regression coefficients are calculated by minimizing the root mean square difference *RMSEb* between the values *RMSE_R* and the corresponding values of the polynomial *RMSE_RA*. The threshold value of the spatial period T_h is calculated as the T_{CR} value at which *RMSE_RA* = 1.

3. Software Implementation of Image Scaling

The software for scaling images by adaptive and combined application of interpolation algorithms was developed in Python [34] based on the mathematical model (1-9). The initial (input) data for the program are digital images f_{RGB} (size $M \times N$ pixels). The initial images are read from graphic files or from a video camera. The color f_{RGB} images are converted to grayscale and recorded in the image f_n (size $M_d \times N_d$ pixels). For each image f_n, the Fourier spectrum F, the energy spectrum P_S, its averaged radial profile P_R and the spatial period T_{CR} are calculated. The direct Discrete Fast Fourier Transform (DFFT) of the image f_n is performed by the fft2() function of the SciPy library.

Adaptive application of interpolation algorithms consists in the fact that the choice of algorithms is performed depending on the value of the spatial period T_{CR} of the image. When $T_{CR} < T_h$, scaling is performed by one of the algorithm complexes, and when $T_{CR} \geqslant T_h$, by another algorithm complex (which provides a smaller scaling error). For example, if bicubic interpolation in the algorithm complex I is used to downscale and upscale of images, and bilinear interpolation in the algorithm complex II is used to downscale and upscale, then the program operation is described by the following activity diagram (Fig. 1). In this case, when $T_{CR} < T_h$, scaling is performed by bilinear interpolation, and when $T_{CR} \geqslant T_h$, by bicubic interpolation.

The scale of the initial f_{RGB} image is downscale by S_c times, i.e. the f_{RGB} image (with size $M \times N$ pixels) is scaled to the f_{RGBs} image (with size $M_s \times N_s$ pixels), where $M_s = S_c \cdot M$. Next, the image is upscale by S_c times, i.e. the f_{RGBs} is scaled to the f_{RGBs2} image (with size $M \times N$ pixels). Scaling of images is performed by the resize() function of the OpenCV library using interpolation methods:

- INTER_LINEAR is a method that implements the bilinear interpolation algorithm;
- INTER_CUBIC is a method that implements the bicubic interpolation algorithm.

The output data (results) of the program are scaled fRGBs2 images.

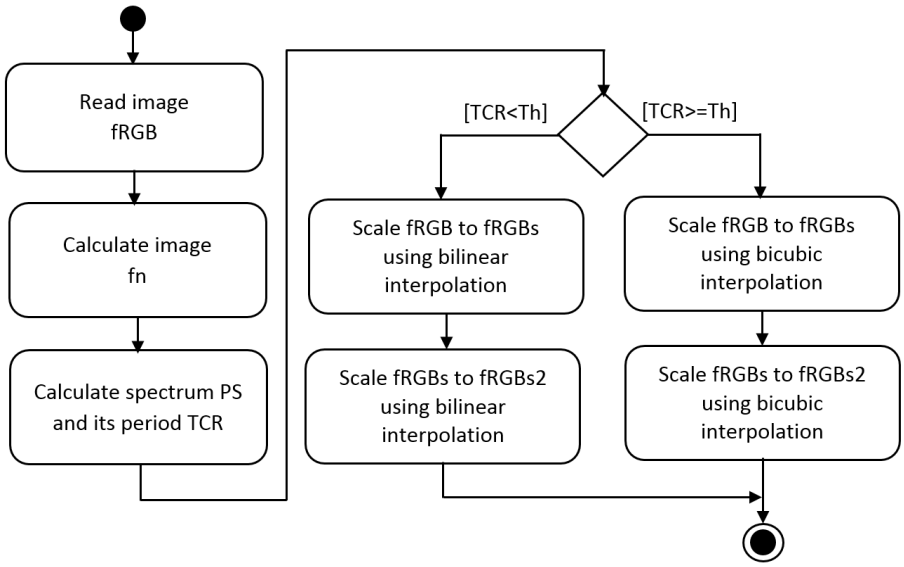


Fig. 1. Activity diagram of a software for scaling images using interpolation algorithms.

4. Results and Discussion

Using the developed program, the following types (subsets) of images were scaled: BSDS300 database images (Fig. 2a), Kikuchi Patterns (Fig. 2b), X-ray biomedical images (Fig. 2c), and text document images (Fig. 2d). In total, the sample contained Q_{Im}=278 images.

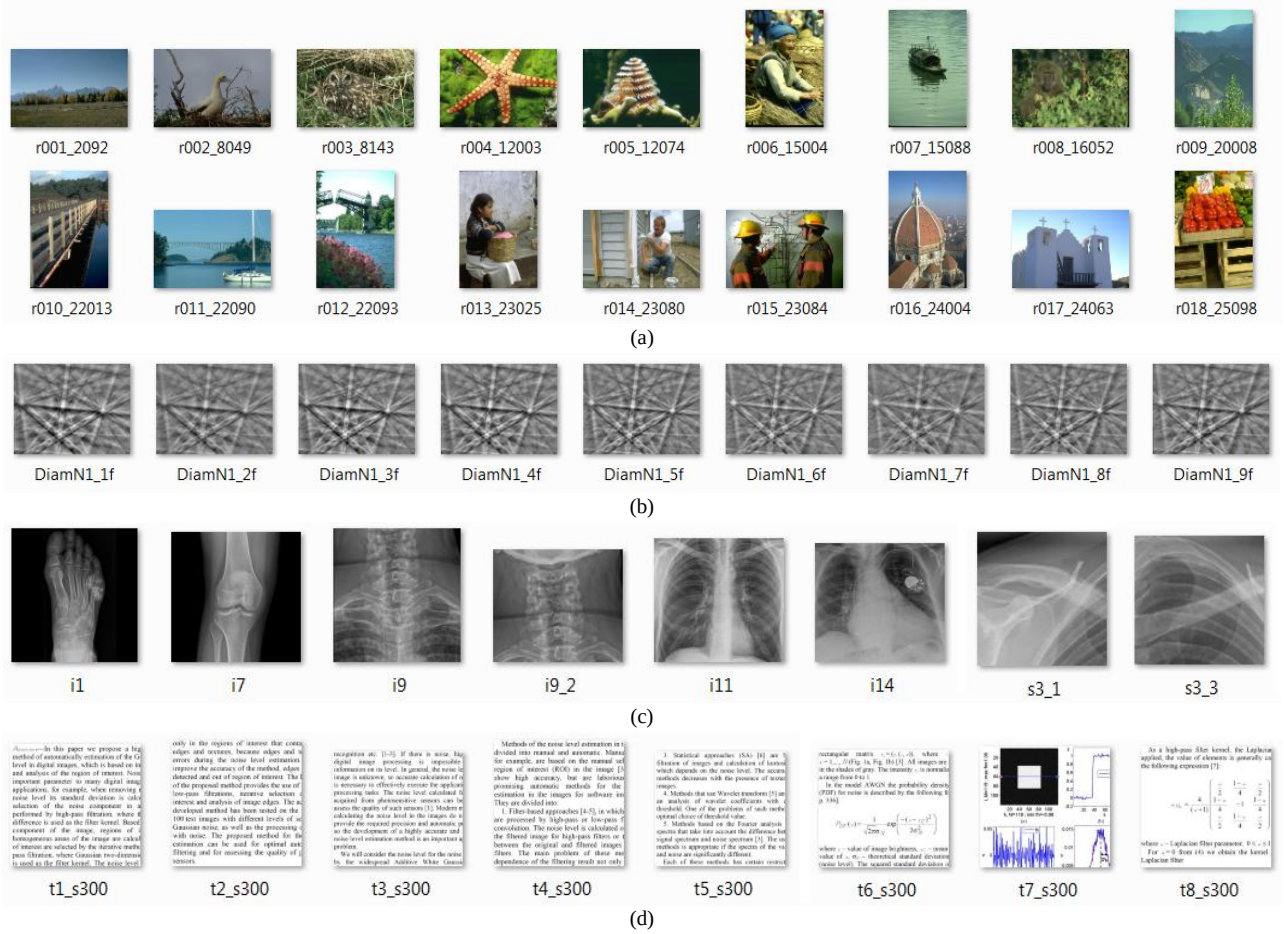


Fig. 2. A fragment of dataset with QIm=278 studied images: a) BSDS300 database images (18 images from 200) [35, 36]; b) Kikuchi Patterns (9 images from 44) [7]; c) X-ray biomedical images (8 images from 17) [37]; d) text document images (8 images from 17) [22].

First, the images were scaled using a set of algorithms I (scale down and up using the bicubic interpolation algorithm) and a set of algorithms II (scale down and up using the bilinear interpolation algorithm).

Let us consider the process of scaling image # 156 from the BSDS300 database [35, 36] (Fig. 3a). From the initial f_{RGB} image, a square image f_n in grayscale is obtained, for which the energy spectrum P_S (Fig. 3b) and the averaged radial profile P_R of the spectrum (Fig. 3c) are calculated. Based on the initial f_{RGB} image, the image f_{RGBs} (Fig. 4a) is calculated in a reduced scale (scale down by 2 times) using bilinear or bicubic interpolation algorithms. By scaling the f_{RGBs} image using bilinear or bicubic interpolation algorithms, the image f_{RGBs2} is calculated in an enlarged scale (Fig. 4b, Fig. 4c, Fig. 4d). In this case, the bicubic interpolation algorithm provides a smaller scaling error *RMSE* (Fig. 4b) than the bilinear interpolation algorithm (Fig. 4c).

The difference between scaled images calculated by different interpolation algorithms is most noticeable in individual fragments of such images (Fig. 5) and on their profiles (Fig. 6). Certain oscillations (ringing artifacts) appear on images scaled by the bicubic interpolation algorithm (Fig. 5c, Fig. 6a). Scaling by the bilinear interpolation algorithm leads to significant image smoothing (Fig. 5d, Fig. 6b). Sequential scaling by the bilinear and bicubic interpolation algorithm (in the case of this image) provides less image distortion due to less blurring (compared to bilinear interpolation) and less oscillations (compared to bicubic interpolation) (Fig. 5e, Fig. 6c).

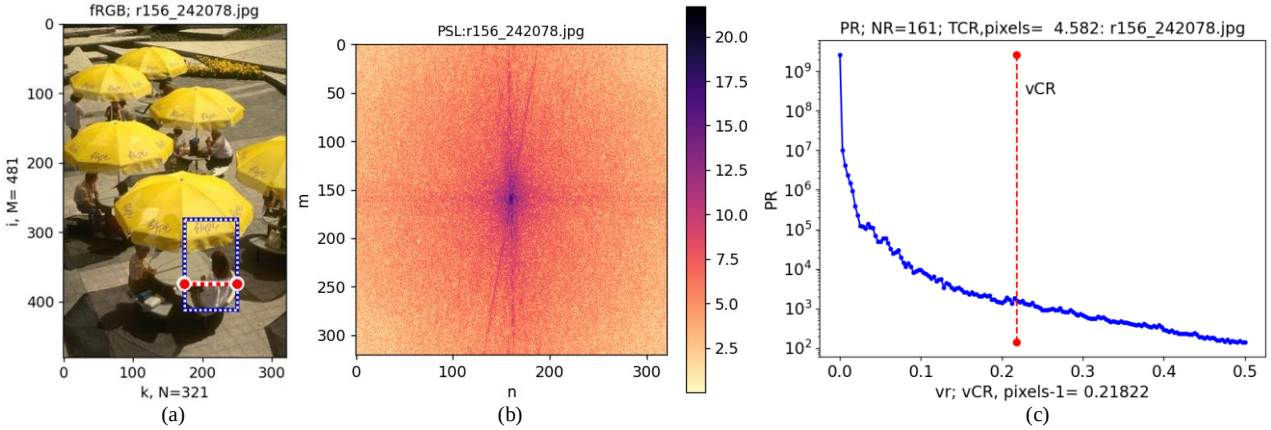


Fig. 3. Initial fRGB image #156 from dataset BSDS300 [34, 35] (a), its energy spectrum PS in logarithmic scale (b) and the averaged radial profile PR of the spectrum (c).

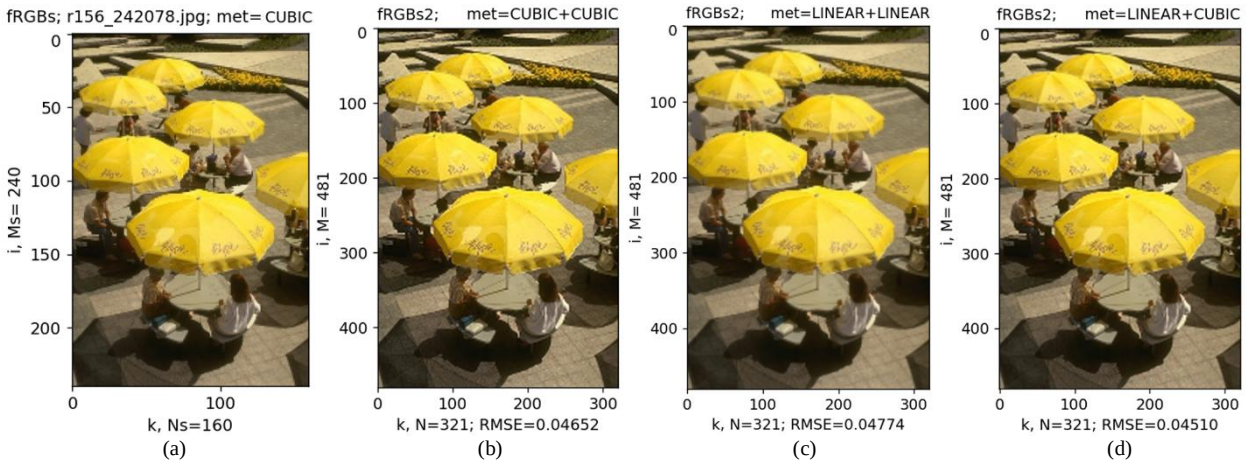


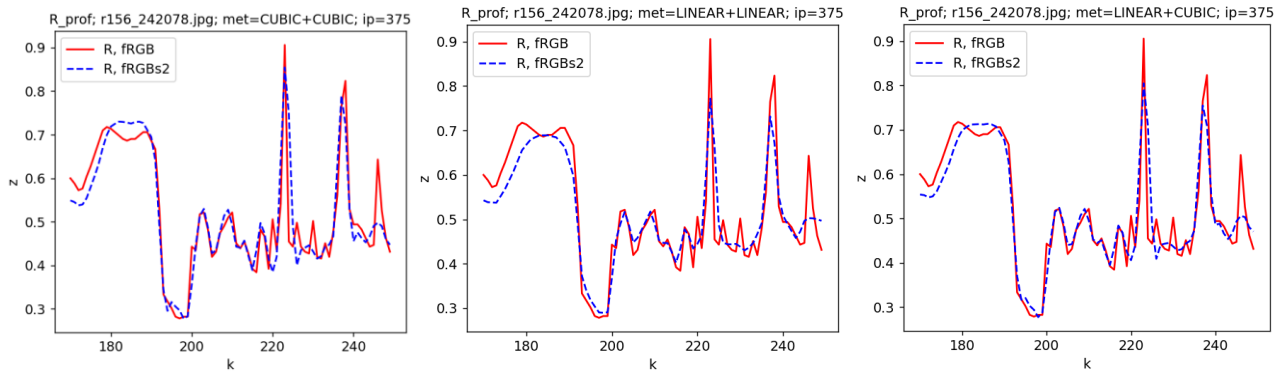
Fig. 4. The fRGBs image in a reduced scale (a) and the fRGBs2 image in an enlarged scale, calculated by the algorithms: (b) bicubic interpolation (algorithm set I, "CUBIC+CUBIC" methods); (c) bilinear interpolation (algorithm set I, "LINEAR+ LINEAR" methods); (d) bilinear and bicubic interpolation ("LINEAR+CUBIC" methods).

For the images of the studied set (Fig. 2), the relative scaling errors *RMSE_R* (8) and the values for their average spatial period T_{CR} (7) were calculated, as a result of which the dependence *RMSE_R* (T_{CR}) was obtained (Fig. 7). The obtained dependence *RMSE_R* (T_{CR}) is described by the regression equation *RMSE_RA* (T_{CR}) (9), namely a polynomial of degree 2. The spatial period threshold value T_h is calculated as the T_{CR} value at which *RMSE_RA* = 1, so T_h = 4.45 pixels (Fig. 7).



(a) (b) (c) (d) (e)

Fig. 5. Image fragments: (a) fRGB (Fig. 3a, fragment highlighted by a rectangle); (b) fRGBs in a reduced scale (Fig. 4a); (c) fRGBs2 in an enlarged scale, “CUBIC+CUBIC” methods (Fig. 4b); (d) fRGBs2 in an enlarged scale, “LINEAR+ LINEAR” methods (Fig. 4c); (e) fRGBs2 in an enlarged scale, “LINEAR+CUBIC” methods (Fig. 4d).



(a) (b) (c)

Fig. 6. Horizontal profiles of the red color channel of the initial fRGB images (Fig. 3a, the ends of the horizontal segment correspond to the beginning and end of the profile) and scaled fRGBs2 images (Fig. 4b, Fig. 4c, Fig. 4d), which are calculated by: (a) bicubic interpolation algorithms (algorithm set I, "CUBIC+CUBIC" methods, RMSE = 0.04652); (b) bilinear interpolation (algorithms set II, "LINEAR+ LINEAR" methods, RMSE = 0.04774); (c) bilinear and bicubic interpolation ("LINEAR+CUBIC" methods, RMSE = 0.4510).

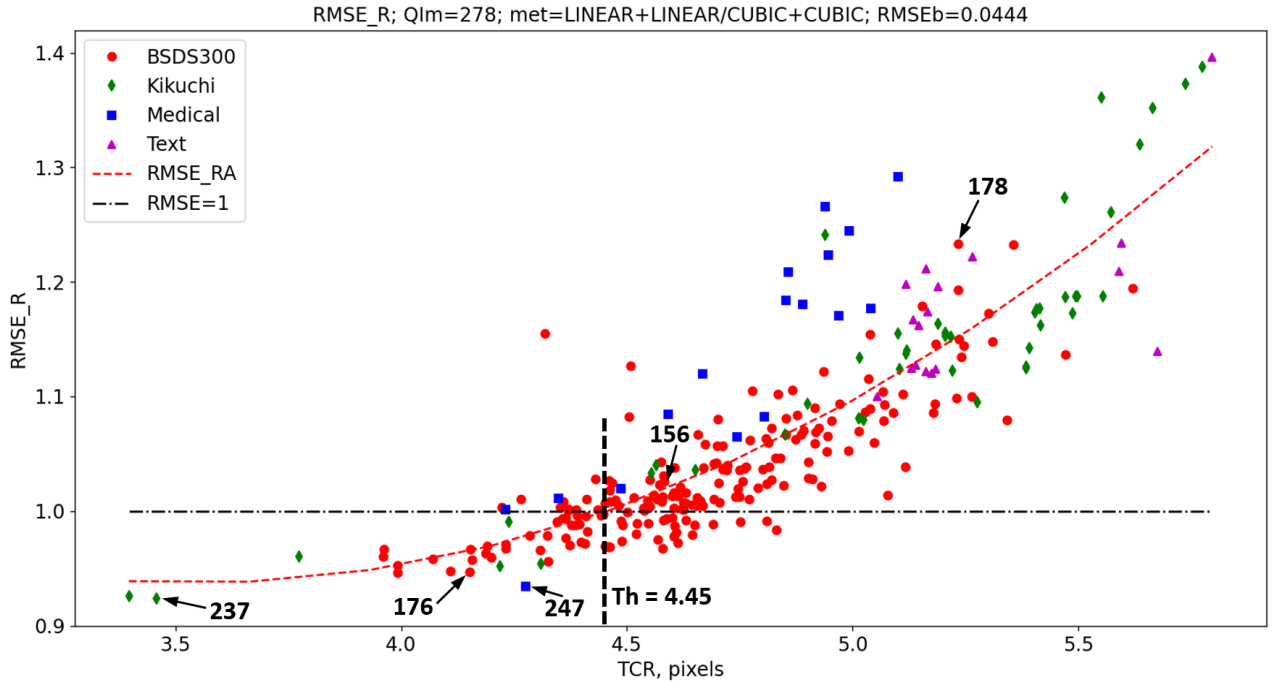


Fig. 7. Dependence of the relative scaling error RMSE_R (8) from the average spatial period TCR (7) for images of the studied dataset (Fig. 2); BSDS300 – images of the BSDS300 database, Kikuchi – images of Kikuchi Patterns, Medical – X-ray biomedical images, Text – images of text documents; RMSE_RA – regression equation (9) (polynomial coefficients b0= 1.876813, b1=-0.530587, b2=0.07490); scaled images were calculated by bicubic interpolation algorithms (algorithms set I, “CUBIC+CUBIC” methods) and bilinear interpolation (algorithms set I, “LINEAR+ LINEAR” methods); numbers 156, 176, 178, 237 and 247 correspond to images in the coordinate space RMSE_R(TCR).

The average spatial frequency of the image v_{CR} (6) and the average spatial period T_{CR} (7) were calculated for the minimum spatial frequency number $d_{min} = [N_R \cdot 0.25]$ and the maximum spatial frequency number $d_{max} = N_R$. Such values of the parameters d_{min} and d_{max} were chosen under the condition of minimizing the root mean square difference *RMSEb* (Fig. 6) between the values of *RMSE_R* and the corresponding values of the polynomial *RMSE_RA* (9).

The results of image scaling by bicubic and bilinear interpolation algorithms show that there is a dependence of the relative scaling error *RMSE_R* from the average spatial period T_{CR}. This dependence is confirmed by the Pearson correlation coefficient *Corr* = 0.843428. Thus, for some images with low $T_{CR} < T_h$ values, the bilinear interpolation algorithm provides a smaller scaling error *RMSE* than the bicubic interpolation algorithm. This scaling feature is observed, for example, for the Kikuchi Patterns # 237 (Fig. 8, Fig. 9) and the X-ray biomedical image # 247 (Fig. 10, Fig. 11).

That is, the image interpolation algorithm can be chosen adaptively according to the criterion of minimizing the scaling error *RMSE*. The proposed method allows to reduce the scaling error, since according to the value of the spatial period T_{CR}, images are divided into two classes: for class # 1 ($T_{CR} \geqslant T_h$), the bicubic interpolation algorithm provides a smaller *RMSE* scaling error, and for class # 2 ($T_{CR} < T_h$), the bilinear interpolation algorithm provides a smaller *RMSE* error (Fig. 7). It is advisable to perform a practical determination of the best algorithm (by the minimum *RMSE*) not through the value of the T_{CR} period (which requires a lot of computing resources), but by comparing rectangular fragments of small size (for example, 64 × 64 pixels) for the original f_{RGB} and scaled f_{RGBs2} images.

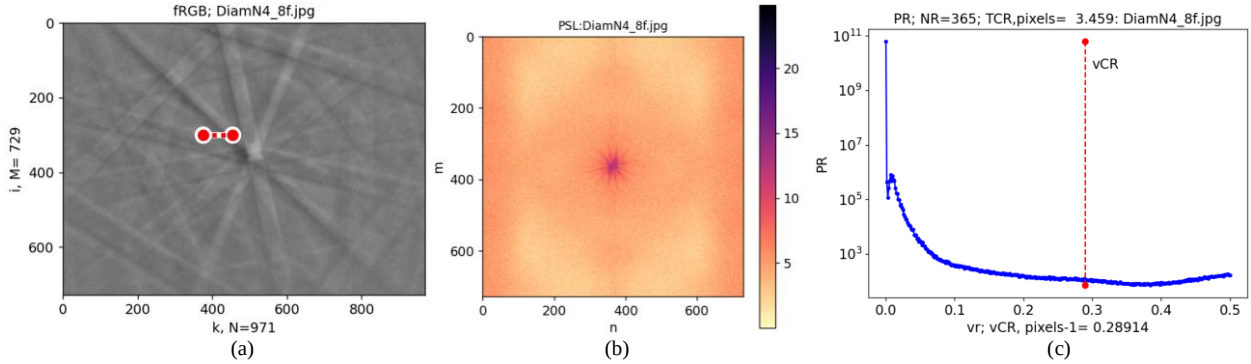


Fig. 8. Initial image fRGB of Kikuchi Patterns # 237 [7] (a), its energy spectrum PS in logarithmic scale (b) and the averaged radial profile PR of the spectrum (c).

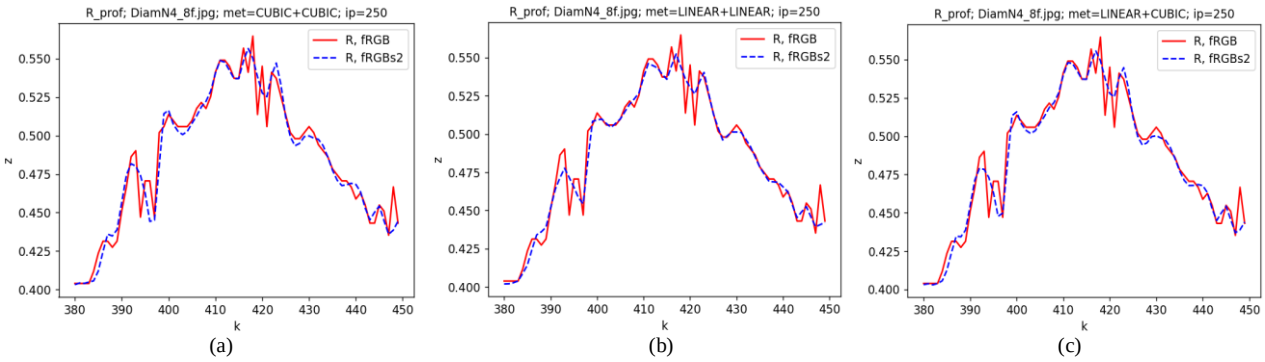


Fig. 9. Horizontal profiles of the red color channel for the fRGB image (Fig. 8a, the ends of the horizontal segment correspond to the beginning and end of the profile) and scaled fRGBs2 images, which are calculated by the algorithms: (a) bicubic interpolation (algorithms set I, "CUBIC+CUBIC" methods, RMSE=0.01637); (b) bilinear interpolation (algorithms set II, "LINEAR+ LINEAR" methods, RMSE=0.01511); (c) bilinear and bicubic interpolation ("LINEAR+CUBIC" methods, RMSE=0.01538).

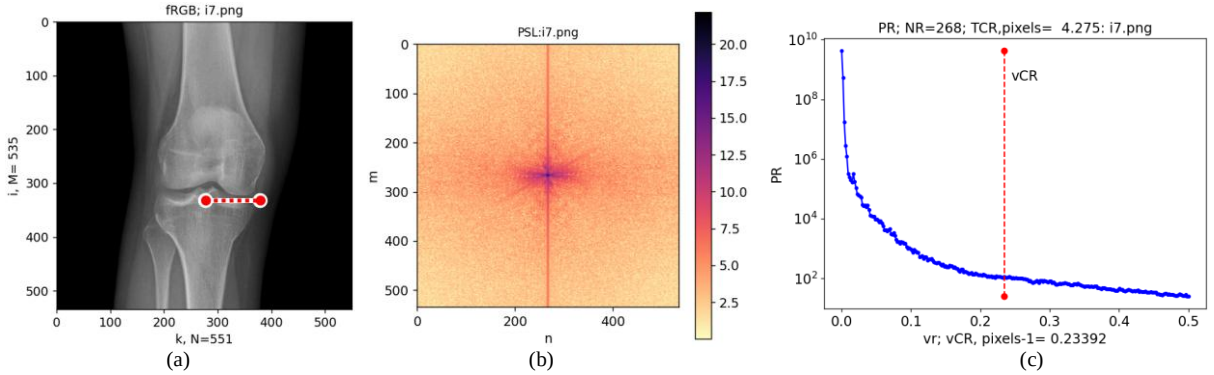


Fig. 10. Initial X-ray biomedical image fRGB # 247 [37] (a), its energy spectrum PS in logarithmic scale (b) and the averaged radial profile PR (c).

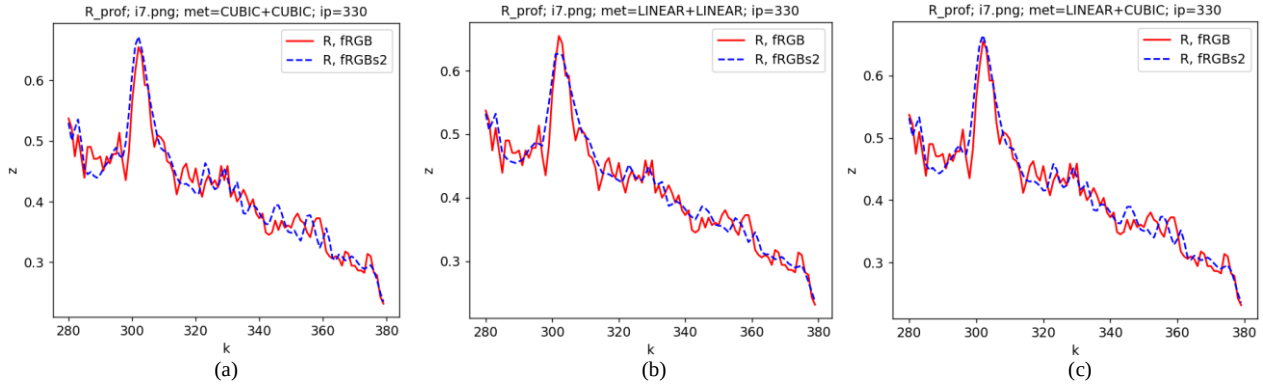


Fig. 11. Horizontal profiles of the red color channel for fRGB images (Fig. 10a) and scaled fRGBs2 images, which are calculated by the algorithms: (a) bicubic interpolation (algorithms set I, "CUBIC+CUBIC" methods, RMSE=0.01147); (b) bilinear interpolation (algorithms set II, "LINEAR+LINEAR" methods, RMSE=0.01072); (c) bilinear and bicubic interpolation ("LINEAR+CUBIC" methods, RMSE=0.01094.

When scaling one image, it is possible to combine different interpolation algorithms. To test the capabilities of this scaling method, images were processed using an algorithm set I (scale down and up using the bicubic interpolation algorithm) and an algorithm set II (scale down using the bilinear interpolation algorithm and scale up using the bicubic interpolation algorithm). As a result of scaling the studied images (Fig. 2), their relative scaling errors *RMSE_R* (8) and average spatial period T_{CR} (7) were calculated (Fig. 12).

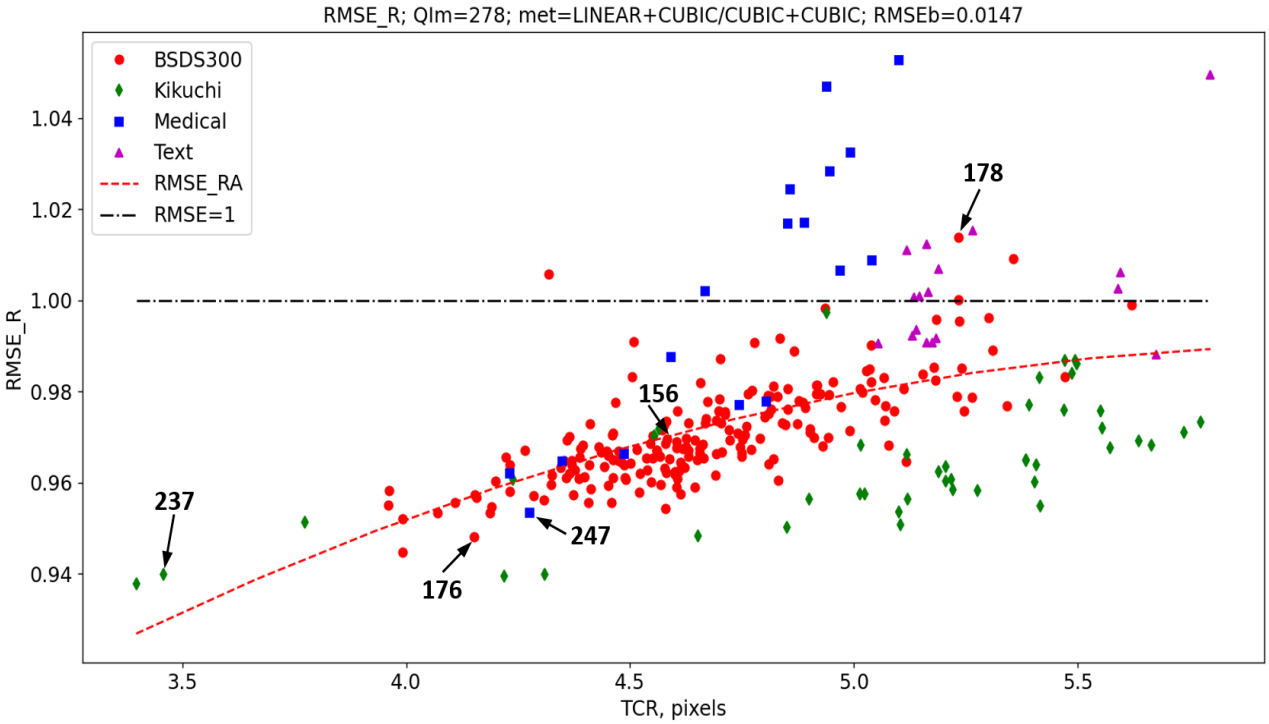


Fig. 12. Dependence of the relative scaling error RMSE_R (8) from the average spatial period TCR (7) of the images of the studied set (Fig. 2); BSDS300 – images of the BSDS300 database, Kikuchi – images of Kikuchi Patterns, Medical – X-ray biomedical images, Text – images of text documents; RMSE_RA – regression equation (9) (polynomial coefficients b0=0.667929, b1=0.105665, b2=-0.008663); scaled images were calculated by bicubic interpolation algorithms (algorithms set I, “CUBIC+CUBIC” methods), bilinear and bicubic interpolation (algorithms set II, “LINEAR+CUBIC” methods); numbers 156, 176, 178, 237, 247 correspond to images in the coordinate space RMSE_R(TCR).

The results of image scaling (Fig. 12) show that there is a correlation between relative scaling error *RMSE_R* and average spatial period T_{CR} (correlation coefficient *Corr* = 0.523043). For most of the studied images, the combined sequential application of the bilinear and bicubic interpolation algorithms (LINEAR+CUBIC) provides a smaller scaling error than the separate application of the bilinear (LINEAR+LINEAR) and bicubic (CUBIC+CUBIC) interpolation algorithms (Table 1).

For example, when scaling image # 156 (Fig. 3, Fig. 4), the smallest *RMSE* error was obtained in the case of sequential application of bilinear and bicubic interpolation algorithms ("LINEAR + CUBIC" methods), which is especially noticeable on the profiles of scaled images (Fig. 6c).

For some images, the smallest *RMSE* error is provided by the bilinear interpolation algorithm, for example, for the Kikuchi Patterns # 237 (Fig. 8, Fig. 9) and for the X-ray biomedical image # 247 (Fig. 10, Fig. 11). This result can be

explained by the presence of a significant level of noise in the images (Fig. 8a, Fig. 10a), since the use of bilinear interpolation leads to smoothing and reduction of the noise component in the image after scaling.

The scaling of the studied images was also performed by the Lanczos algorithm (LANCZOS+LANCZOS) and by combining bilinear interpolation with the Lanczos algorithm (LINEAR+LANCZOS) (Table 1). However, when processing images by reducing and increasing the scale, the Lanczos algorithm provides a greater error (compared to the combination of bilinear and bicubic interpolation), and at the same time has a lower speed. Therefore, for such image scaling, it is more expedient to sequentially use bilinear and bicubic interpolation.

The hypothesis of a normal distribution of *RMSE* values when scaling images of the studied dataset was confirmed by the Pearson χ^2 criterion [38]. Based on the scaling results for each set of interpolation algorithms, the average scaling error A_R and the standard deviation σ_R for *RMSE* were calculated, and the limits of the confidence interval $A_{Rmin} < A_R < A_{Rmax}$ with a reliability of $\gamma = 0.95$ were also calculated [38] (Table 1, Fig. 13).

Table 1. Average scaling error A_R and standard deviation σ_R for *RMSE* values, confidence interval limits $A_{Rmin} < A_R < A_{Rmax}$ for a dataset of $Q_{Im} = 278$ images (Fig. 2).

	CUBIC+CUBIC	LINEAR+LINEAR	LINEAR+CUBIC	LANCZOS+LANCZOS	LINEAR+LANCZOS
A_R	0.03624219	0.03787999	0.03530453	0.03848144	0.03555926
σ_R	0.02402492	0.0255262	0.02351924	0.02548071	0.02363227
A_{Rmin}	0.03341799	0.03487931	0.03253977	0.03548752	0.03278256
A_{Rmax}	0.03906639	0.04088067	0.03806929	0.04147654	0.03833612

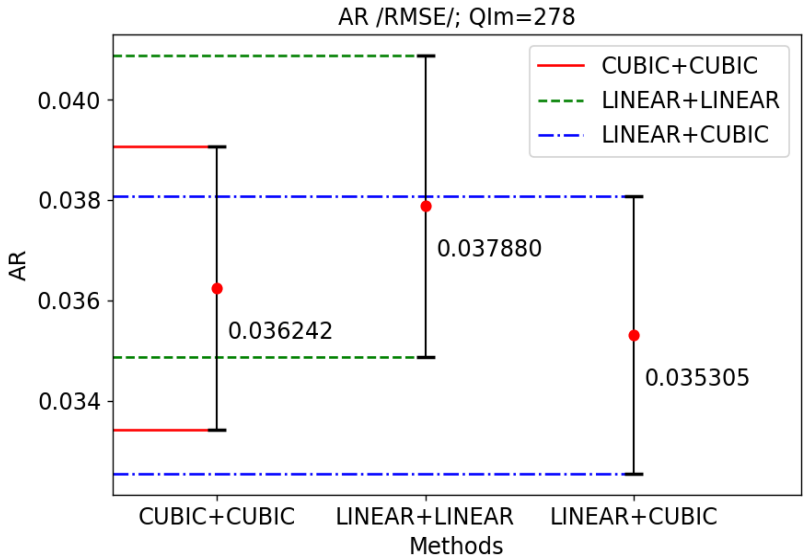


Fig. 13. Average scaling errors A_R and their confidence interval limits for a series of $Q_{Im} = 278$ images (Fig. 2).

Thus, according to the average scaling error A_R and taking into account the limits of its confidence interval A_{Rmin}, A_{Rmax}, the smallest scaling error is provided by the set of bilinear and bicubic interpolation algorithms (LINEAR+CUBIC), the average value is obtained for the bicubic interpolation algorithm (CUBIC+CUBIC), and the highest error is given by the bilinear interpolation algorithm (LINEAR+LINEAR). This result confirms the effectiveness of the combined application of interpolation algorithms. However, the obtained regularities for scaling errors were obtained sequentially when reducing the image scale by 2 times and then increasing the scale by 2 times. If the image scale is first increased, then a smaller error is obtained in most cases when using the bicubic interpolation algorithm. A series of 278 images was also processed with scaling factor 3 (reduction and increase). As in the case of scaling factor 2, the smallest scaling error was obtained with the sequential application of bilinear and bicubic interpolation algorithms.

5. Conclusion and Future Research Directions

The possibilities of increasing the accuracy of scaling digital images using bilinear and bicubic interpolation algorithms were investigated. Scaling errors were estimated through the root mean square error (*RMSE*) between the brightness of pixels of the original and scaled images. Scaling of images using interpolation algorithms and analysis of the obtained results were implemented programmatically in Python. Scaling of a dataset of $Q_{Im} = 278$ images of different types was performed: images of the BSDS300 database and Kikuchi Patterns, X-ray biomedical images and images of text documents. Image processing consisted of scaling images using a set of two interpolation algorithms, namely, scale down by 2 times using algorithm # 1 and subsequently scale up by 2 times using algorithm # 2. Such processing is appropriate, in particular, for reducing the volume of data transmitted in telecommunication systems.

The influence of the average spatial period T_{CR} of the image on the relative scaling error *RMSE_R*, which is equal to the ratio of the *RMSE* error for different interpolation algorithms, is analyzed. The period T_{CR} is calculated based on the radial profile P_R for the energy spectrum P_S of the image. It is established that the dependence of the relative scaling error *RMSE_R* from the values of the spatial period T_{CR} of the images is described by a regression equation in the form of a polynomial of degree 2.

A significant correlation was obtained between the values of the relative scaling error *RMSE_R* and the spatial period T_{CR} of images scaled by the bicubic and bilinear interpolation algorithms. In most cases, the bicubic interpolation provides a smaller scaling error *RMSE*, but for some images with small values of the period T_{CR}, the bilinear interpolation provides a smaller *RMSE* error. Therefore, it is proposed to increase the scaling accuracy by adaptively selecting the interpolation algorithm for each image according to the criterion of minimizing the scaling error.

The feasibility of combined use of interpolation algorithms are shown, which consists in successive scaling of one image by different interpolation algorithms. A statistical analysis of the scaling results is carried out, the average scaling error A_R and the standard deviation σ_R for *RMSE* values are calculated, and the limits of the confidence interval $A_{Rmin} < A_R < A_{Rmax}$ with reliability γ are also calculated. According to the results of statistical analysis, it is established that scaling down by the bilinear interpolation algorithm and scaling up by the bicubic interpolation algorithm in most cases provides a smaller error than the separate use of the bicubic and bilinear interpolation algorithms.

In future studies, for the highest quality image scaling, it is planned to use more complex interpolation algorithms and artificial neural networks, in particular, CNN. The proposed interpolation method can be used to calculate input images of the desired size for the SRCNN [16] and SR3 [17] methods (in which images are scaled to the desired size by the bicubic interpolation), which will allow images with fewer defects to be fed to the inputs of neural networks and ensure higher accuracy of the resulting images. The proposed method can also be implemented in telecommunication systems for transmitting images at a reduced scale and for restoring the original sizes of images.

Author Contributions Statement

Serhiy Balovsyak – Methodology, and Supervision: Proposed research ideas, Development of a mathematical model, Constructed the overall framework, and supervised project execution.

Mariana Borcha – Data Curation: Handled data acquisition, dataset preprocessing; Contributed to the literature survey.

Yurii Hnatiuk – Conceptualization: Proposed research ideas, Development of a mathematical model; Software Implementation and Statistical Analysis; Writing – Drafted the initial manuscript, contributed to the literature survey, and documented the technical background of the study.

Khrystyna Odaiska – Formal Analysis, Visualization: Performed in-depth analysis of experimental results.

Ihor Fodchuk – Writing – Review and Editing, and Project Management: Reviewed and edited the manuscript, ensured clarity and coherence, and helped coordinate project milestones and deadlines.

All authors have read and agreed to the published version of the manuscript.

Conflict of Interest

The authors declare no conflict of interest.

Funding Declaration

This research was not supported by a grant.

Data Availability Statement

This study analyzed publicly available datasets. The datasets can be found here: The Berkeley Segmentation Dataset and Benchmark. BSDS300, URL: https://www2.eecs.berkeley.edu/Research/Projects/CS/vision/bsds/ (Last accessed: 21.02.2025)

Ethical Declarations

Statements of ethical approval for studies involving human subjects and/or animals.

Acknowledgment

We would like to express our gratitude to the reviewers for their precise and succinct recommendations that improved the presentation of the results obtained.

Declaration of Generative AI in Scholarly Writing

AI and AI-assisted technologies were not used during the writing process.

Abbreviations

The following abbreviations are used in this manuscript:

ANN - Artificial Neural Networks
CNN - Convolutional Neural Networks
DFFT - Discrete Fast Fourier Transform
DFT - Discrete Fourier Transform
ESRGAN - Enhanced Super-Resolution Generative Adversarial Network
MBRHAB - Multi-Branch Residual Hybrid Attention Block
MSE - Mean Square Error
PSNR - Peak Signal to Noise Ratio
RMSE - Root Mean Square Error
SNN - Spiking Neural Network
SRCNN - Super-Resolution Convolutional Neural Network
SSIM - Structural Similarity Index

References

[1] R. Gonzalez, and R. Woods, *Digital image processing*. 4th edidion, Pearson/ Prentice Hall, NY, 2018.
[2] M. Dixit, and R.N. Yadav, "A Review of Single Image Super Resolution Techniques using Convolutional Neural Networks," *Multimedia Tools and Applications*, vol. 83, pp. 29741–29775, 2024. doi: 10.1007/s11042-023-16786-9.
[3] S. Palani, *Principles of Digital Signal Processing*. Springer Cham. 2022.
[4] M. Peyvasteh, L. Tryfonyuk, V. Ushenko, A.-V. Syvokorovskaya, A. Dubolazov, O. Vanchulyak, A. Ushenko, Yu. Ushenko, M. Gorsky, M. Sidor, Yu. Tomka, I. Soltys, A. Bykov, and I. Meglinski, "3D Mueller-matrix-based azimuthal invariant tomography of polycrystalline structure within benign and malignant soft-tissue tumours," *Laser Physics Letters*, vol. 17 (115606), pp. 1-9, 2020. doi: 10.1088/1612-202X/abbee0.
[5] O. Berezsky, P. Liashchynskyi, O. Pitsun, P. Liashchynskyi, and M. Berezkyy, "Comparison of Deep Neural Network Learning Algorithms for Biomedical Image Processing," *CEUR Workshop Proceedings*, pp. 135–145, 2022.
[6] S. Balovsyak, I. Fodchuk, Kh. Odaiska, Yu. Roman, and E. Zaitseva, "Analysis of X-Ray Moir éImages Using Artificial Neural Networks," *IntelITSIS 2022: 3nd International Workshop on Intelligent Information Technologies and Systems of Information Security, March 23–25, 2022, Khmelnytskyi, Ukraine, CEUR Workshop Proceedings*, pp. 187-197, 2022.
[7] I. Fodchuk, S. Ivakhnenko, V. Tkach, S. Balovsyak, M. Borcha, N. Solodkii, I. Gutsulyak, A. Kuzmin, and O. Sumaryuk, "Local strain distribution in synthetic diamond crystals, determined by the parameters of the energy spectrum of the Kikuchi patterns," *Journal of Superhard Materials*, vol. 42, no. 1, pp. 1-8, 2020. doi: 10.3103/S1063457620010049.
[8] O.V. Derevyanchuk, H. O. Kravchenko, Y.V. Derevianchuk, and V.V. Tomash, "Recognition images of broken window glass," *Proceedings of SPIE*, vol. 12938, pp. 12938C-1 – 12938C-4, 2024. doi: 10.1117/12.3012995.
[9] R. Kvyetnyy, V. Kotsiubynskyi, O. Kyrylenko, O. Kolesnytskyj, V. Dumenko, A. Kotyra, D. Mussayeva, and N. Abilkaiyr, "Using multiple optical cameras for correspondence identification between objects in the fields of view," *Proceedings of SPIE* "Optical Fibers and Their Applications 2023", vol. 12985, pp. 129850A-1 – 129850A-6, 2023. doi: 10.1117/12.3022791.
[10] W. Burger, and M.J. Burge, "Geometric Operations," in *Digital Image Processing. Texts in Computer Science*, Springer, Cham., 2022, pp 601–637. doi: 10.1007/978-3-031-05744-1_21.
[11] B. Crnković, J. Škifić, and T. Bosner, "WENO based adaptive image zooming algorithm," *Applied Mathematics and Computation*, vol. 492, 129228, 2025. doi: 10.1016/j.amc.2024.129228.
[12] P. Radiuk, O. Barmak, E. Manziuk, and Iu. Krak, "Explainable Deep Learning: A Visual Analytics Approach with Transition Matrices," *Mathematics*, vol. 12 (1024), pp. 1-32, 2024. doi: 10.3390/math12071024.
[13] F. Sun, and W. Song, "A Super-Resolution and 3D Reconstruction Method Based on OmDF Endoscopic Images," *Sensors*, vol. 24 (15), 4890, 2022. doi: 10.3390/s24154890.
[14] K.-L. Chung, and D.-Y. Row, "An Adaptive Joint Bilateral Interpolation-Based Color Blending Method for Stitched UAV Images," *Remote Sensing*, vol. 14 (21), 5440, pp. 1-19, 2022. https://doi.org/10.3390/rs14215440.
[15] Z. Cheng, "Research on Image Up-scaling and Super-resolution Based on Convolutional Neural Network," *Highlights in Science, Engineering and Technology*, vol. 72, pp.1258-1263, 2023. doi: 10.54097/ef4k8k08.
[16] C. Dong, C.C. Loy, K. He, and X. Tang, "Learning a Deep Convolutional Network for Image Super-Resolution," *Computer Vision – ECCV 2014. Lecture Notes in Computer Science, Springer, Cham*., vol. 8692, pp. 184-199, 2014. doi: 10.1007/978-3-319-10593-2_13.
[17] C. Saharia, J. Ho, W. Chan, T. Salimans, D. J. Fleet and M. Norouzi, "Image Super-Resolution via Iterative Refinement," in *IEEE Transactions on Pattern Analysis and Machine Intelligence*, vol. 45, no. 4, pp. 4713-4726, 2023. doi: 10.1109/TPAMI.2022.3204461.

[18] G. Li, Zh. Zhou, G. Wang, "A joint image super-resolution network for multiple degradations removal via complementary transformer and convolutional neural network," *IET Image Processing*, vol. 18, no. 5, pp. 1344-1357. 2024. doi: 10.1049/ipr2.13030.
[19] Y. Xu, T. Guo, C. Wang, "A Remote Sensing Image Super-Resolution Reconstruction Model Combining Multiple Attention Mechanisms," *Sensors*, vol. 24 (14), 4492, pp.1-17, 2024. doi: 10.3390/s24144492.
[20] K. Mahmut, "Image interpolation with spiking neural network based pixel similarity," *Signal, Image and Video Pro*cessing, vol. 18, pp. 6925–6936, 2024. doi: 10.1007/s11760-024-03362-3.
[21] Waifu2x, URL: https://waifu2x.udp.jp/index.uk.html (Last accessed: 23.12.2024).
[22] S. V. Balovsyak, O. V. Derevyanchuk, I. M. Fodchuk, O. P. Kroitor, Kh. S. Odaiska, O. O. Pshenychnyi, A. Kotyra, and A. Abisheva, "Adaptive oriented filtration of digital images in the spatial domain," *Proceedings of SPIE*, vol. 11176, 111761A-1 – 111761A-6, 2019. doi: 10.1117/12.2537165.
[23] L. Khvostivska, M. Khvostivskyi, I. Dediv, V. Yatskiv, and Y. Palaniza "Method, Algorithm and Computer Tool for Synphase Detection of Radio Signals in Telecommunication Networks with Noises," *CEUR Workshop Proceedings*, pp. 173–180, 2023.
[24] J.-W. Han, J.-H. Kim, S.-H. Cheon, J.-O. Kim and S.-J. Ko, "A novel image interpolation method using the bilateral filter*,"* in *IEEE Transactions on Consumer Electronics*, vol. 56, no. 1, pp. 175-181, 2010. doi: 10.1109/TCE.2010.5439142.
[25] A.L. Bovik, *The Essential Guide to Image Processing*, Elsevier Inc., 2009.
[26] Y. Zuo, W. Yao, Y. Hu, Y. Fang, W. Liu and Y. Peng, "Image Super-Resolution via Efficient Transformer Embedding Frequency Decomposition With Restart*,"* in *IEEE Transactions on Image Processing*, vol. 33, pp. 4670-4685, 2024, doi: 10.1109/TIP.2024.3444317.
[27] S. Krigg, *Computer Vision Metrics. Survey, Taxonomy, and Analysis*, Apress Berkeley, CA, 2014.
[28] R. Archana, and P.S.E. Jeevaraj, "Deep learning models for digital image processing: a review," *Artif. Intell. Rev.*, vol. 57 (11), pp. 1-33, 2024. doi: 10.1007/s10462-023-10631-z.
[29] W. Burger, and M.J. Burge, "The Discrete Fourier Transform in 2D," in *Digital Image Processing. Texts in Computer Science*, Springer, Cham., 2022, pp. 567–587. doi: 10.1007/978-3-031-05744-1_19.
[30] S. Sharma, and T. Varma, "Discrete combined fractional Fourier transform and its application to image enhancement," *Multimed. Tools Appl.*, vol. 83, pp. 29881–29896, 2024. doi: 10.1007/s11042-023-16742-7.
[31] A. Brostrom, and K. Molhave, "Spatial Image Resolution Assessment by Fourier Analysis (SIRAF)," *Microscopy and Microanalysis*, vol. 28, no. 2, pp. 469–477, 2022. doi: 10.1017/S1431927622000228.
[32] M. D. Borcha, A. V. Zvyagintseva, V. M. Tkach, K. A. Yushchenko, S. V. Balovsyak, I. M. Fodchuk, and V. Yu. Khomenko, "Local Deformations in the Vicinity of Welded-Joint Crack of Nickel Alloy Determined with Use of Fourier Transform of the Kikuchi Patterns," *Metallofizika i Noveishie Tekhnologii*, vol. 35, pp. 1359-1370, 2013.
[33] S. Thonhpanja, A. Phinyomark, P. Phukpattaranont, and C. Limsakul, "Mean and Median Frequency of EMG Signal to Determine Muscle Force based on Time-dependent Power Spectrum," *Electronika IR Elektrotechnika*, vol. 19, no. 3, pp. 51-56, 2013. doi: 10.5755/j01.eee.19.3.3697.
[34] G. Guillen, "Digital Image Processing with Python and OpenCV," in *Sensor Projects with Raspberry Pi. Maker Innovations Series*, Apress, Berkeley, CA, 2024, pp.105–147. doi: 10.1007/979-8-8688-0464-9_5.
[35] C. Fowlkes, D. Martin, and J. Malik, "Local Figure/ Ground Cues are Valid for Natural Images," *Journal of Vision*, vol. 7(8), no. 2, pp. 1-9, 2007.
[36] The Berkeley Segmentation Dataset and Benchmark. BSDS300, URL: https://www.eecs.berkeley.edu/Research/Projects/CS/vision/bsds (Last accessed: 21.12.2024).
[37] S. Balovsyak, M. Borcha, M. Gregus ml., Kh. Odaiska, and N. Serpak, "Automatic Processing of Digital X-ray Medical Images by Bilateral Filtration Method*," IntelITSIS 2021, March 24–26, 2021. Khmelnytskyi, Ukraine, CEUR Workshop Proceedings*, pp. 280-294, 2021.
[38] O. Knill, *Probability and Stochastic. Processes with Applications*. Overseas Press (India), Pvt. Ltd, 2009.

Authors' Profiles



Serhiy Balovsyak: Graduated from Chernivtsi State University (1995). In 2018, he defended his doctoral dissertation in the specialty "Computer systems and components".

Currently position – associate professor at the Department of Computer Systems and Networks of Yuriy Fedkovych Chernivtsi National University, Ukraine.

Research Interests: digital processing of signals and images, programming, pattern recognition, artificial neural networks.



Mariana Borcha: Graduated from Chernivtsi State University (1992). Doctor of Physics and Mathematics Sciences (2014).

Currently position – Head of Department of Information Technologies and Computer Physics of Yuriy Fedkovych Chernivtsi National University, Ukraine.

Research Interests: material science, semiconductors, alloys, structure deformation and defects, X-ray diffraction, digital processing of signals and images.



Yurii Hnatiuk: Graduated from Chernivtsi National University (2019) with a degree in "Computer Engineering". In 2022, entered postgraduate studies in the specialty "Telecommunications and radio engineering".

Research interests include digital signal and image processing, programming, artificial neural networks.



Khrystyna Odaiska: In 2013, graduated from Chernivtsi National University with a degree in Computer Engineering (master's level). In 2020, defended her PhD thesis in the specialty "Computer systems and components".

Currently position – assistant professor at the Department of Computer Systems and Networks of Chernivtsi National University.

Research Interests: digital image processing, programming, data base, computer graphics.



Ihor Fodchuk: In 1979 graduated from Chernivtsi State University. In 1994 defended Doctoral thesis in the specialty “Solid State Physics” and in 1996 become Professor of Chernivtsi State University.

Currently he is a Head of Department of Urban Planning and Urbanism of Yuriy Fedkovych Chernivtsi National University, Ukraine.

Research interests include solid state physics, structure deformation and defects, X-ray diffraction, material structure diagnostics, digital signal processing of experimental data.

How to cite this paper: Serhiy Balovsyak, Mariana Borcha, Yurii Hnatiuk, Khrystyna Odaiska, Ihor Fodchuk, "Scaling of Digital Images by Adaptive and Combined Application of Interpolation Algorithms", International Journal of Image, Graphics and Signal Processing(IJIGSP), Vol.18, No.2, pp. 36-50, 2026. DOI:10.5815/ijigsp.2026.02.03